Effect of Tb^{3+} concentration on the optical and vibrational properties of YBO_3 tri-doped with Eu^{3+}, Ce^{3+}, and Tb^{3+}

S. Sohal,[1] M. Nazari,[2] X. Zhang,[3] E. Hassanzadeh,[1] V. V. Kuryatkov,[4] J. Chaudhuri,[3] L. J. Hope-Weeks,[5] J. Y. Huang,[1] and M. Holtz[2,a)]
[1]*Department of Physics, Texas Tech University and Nano Tech Center, Lubbock, Texas 79409, USA*
[2]*Department of Physics, Texas State University, San Marcos, Texas 78666, USA*
[3]*Department of Mechanical Engineering, Texas Tech University, Lubbock, Texas 79409, USA*
[4]*Department of Electrical and Computer Engineering and Nano Tech Center, Texas Tech University, Lubbock, Texas 79409, USA*
[5]*Department of Chemistry and Biochemistry, Texas Tech University, Lubbock, Texas 79409, USA*

(Received 6 April 2014; accepted 29 April 2014; published online 9 May 2014)

Structural and optical studies are reported of yttrium orthoborate YBO_3 when tri-doped with Eu^{3+}, Ce^{3+}, and Tb^{3+}, focusing on the role of terbium concentration. Incorporation of Tb^{3+} affects emission properties for photoluminescence (PL) excited by near ultraviolet light. For constant cerium and europium concentrations, increasing the Tb^{3+} results in diminished PL from the Ce^{3+} and Tb^{3+} color centers. Simultaneously, the PL excitation bands related to both Ce^{3+} and Tb^{3+} increase in intensity for red emission from the Eu^{3+}. Results are consistent with a $Ce^{3+} \rightarrow (Tb^{3+})_n \rightarrow Eu^{3+}$ energy transfer scheme, where $(Tb^{3+})_n$ denotes a chain incorporating n terbium ions. A high red to orange PL intensity ratio is obtained, ranging from 1.34 to 2.09. Raman vibrational bands show a systematic change, with Tb^{3+} concentration, in the B_3O_9 ring terminal oxygen bending mode coordinated with the yttrium site where dopant ions substitute. The structural changes are interpreted as variations in the local neighborhood of these sites in the YBO_3:Ce^{3+},Tb^{3+},Eu^{3+} crystal structure.
 [http://dx.doi.org/10.1063/1.4875914]

I. INTRODUCTION

Phosphors exhibiting narrow emission in the red wavelength range are needed for improving the color-rendering index (CRI) of white light emitting diodes (WLEDs).[1,2] Emission from YBO_3:Eu^{3+} is attractive for solid state lighting applications due to its narrow red emission bands at wavelengths 611 and 627 nm. However, the weak and narrow *f–f* transitions of Eu^{3+} ions in the near ultraviolet (UV) to blue range are problematic for application in phosphor-based WLEDs due to the need for strong absorption of the emission from InGaN-based LEDs. This has motivated research to incorporate dopants for sensitizing these color centers to increase the photoluminescence (PL) efficiency with near UV and blue pumping wavelengths.

Recently, utilizing energy transfer (ET) mechanisms from $Ce^{3+} \rightarrow Tb^{3+}$ and $Tb^{3+} \rightarrow Eu^{3+}$, the Ce^{3+}-$(Tb^{3+})_n$-Eu^{3+} (where n corresponds to the number of Tb^{3+} ions in a representative energy migration chain) combination has been shown to increase the luminescence efficiency of Eu^{3+} emission in the YBO_3 host matrix using near UV excitation.[2] The concentration of Tb^{3+} ions plays a crucial role in the $Ce^{3+} \rightarrow Tb^{3+} \rightarrow Eu^{3+}$ energy transfer and acts as a good intermediate to minimize the competing metal-metal charge transfer (MMCT) quenching between Ce^{3+} and Eu^{3+} ions in YBO_3, which reduces the red emission intensity. Despite improvement in luminescence efficiency of YBO_3:Ce^{3+},Tb^{3+},Eu^{3+}, this phosphor shows poor chromaticity due to intense orange (O at wavelength 591 nm) and weak red (R at 611 and 627 nm) emission of Eu^{3+}. The orange emission is a magnetic dipole parity allowed process, while red emission is an electric dipole parity forbidden process. According to Judd–Ofelt theory, reduced local site-symmetry in the Eu^{3+} ion neighborhood is one factor for increasing chromaticity.[3,4] Perturbation of the Eu^{3+} color center symmetry in the host matrix may mix states which allow the electric dipole process to participate in the emission process. Because there are few ways to examine the local order of Eu^{3+} ions in YBO_3 host matrix, this has not yet been fully studied. In a previous paper,[5] we reported changes in the PL and Raman spectra for YBO_3:Eu^{3+} grown under different conditions. That work focused on the terminal oxygen stretching (TS) vibration, but changes were also observed in the terminal bending (TB) mode. Those changes were linked with crystal distortion near the color center and resulting changes in the PL interpreted according to Judd-Ofelt theory.

Combined photoluminescence emission and excitation (PL and PLE, respectively) spectroscopic studies are powerful for obtaining information about energy transfer between impurities. Excitation of one impurity and emission from another supports identification of energy transfer. Concentrations may then be systematically varied to determine conditions most conducive to the desired transfer for improving the PL efficiency related to a particular excitation.

Here, we examine the effect of Tb^{3+} ions on the structural order near Eu^{3+} ions and its impact on emission properties of YBO_3:Ce^{3+},Tb^{3+},Eu^{3+}. We synthesize the materials using the hydro(solvo)thermal method. This approach

a)Author to whom correspondence should be addressed. Electronic mail: mark.holtz@txstate.edu

permits control of several parameters in the synthesis process and allows a range of impurity doping approaches. We previously used this method to produce different morphologies of $YBO_3:Eu^{3+}$.[6] The materials show improved chromaticity for excitation in the near UV region. Here, we extend this approach to grow $YBO_3:Ce^{3+},Tb^{3+},Eu^{3+}$ for improving red phosphors with near UV optical pumping. We investigate structural changes in the host matrix with increasing concentration of Tb^{3+} ions using x-ray diffraction (XRD) and Raman spectroscopy, and the impact on optical properties using PL and PLE. Results are consistent with an energy transfer mechanism from Ce^{3+} to Eu^{3+} mediated by the Tb^{3+} ions.

II. EXPERIMENTAL DETAILS

The samples were synthesized from precursors $Y(NO_3)_3{\cdot}6H_2O$ and $K_2B_4O_7{\cdot}4H_2O$ by the hydro(solvo)thermal technique without any organic solvent or surfactant.[6] A 1:2 molar ratio was selected for the Y and B starting precursors and a 1:1 mixture of deionized (DI) water and ethanol solvents was used in the synthesis process. Aqueous solution of 0.2 M (each) $Y(NO_3)_3{\cdot}6H_2O$, $Ce(NO_3)_3{\cdot}6H_2O$, $Eu(NO_3)_3{\cdot}6H_2O$, and $Tb(NO_3)_3{\cdot}5H_2O$ were mixed together with the water and ethanol under vigorous stirring. The samples are designated according to the volumes of each dopant precursor used in the synthesis. A dopant molar concentration of 0.2% was used for Ce^{3+} and the Eu^{3+} ion molar concentrations were fixed at 1% and 5%. The Tb^{3+} ion concentration was varied from 5% to 50%. An aqueous solution of 0.2 M $K_2B_4O_7{\cdot}4H_2O$ was added to the former solution while stirring. The white precipitate appeared immediately. The pH was fixed at ~8.5 using 1 M ammonia water. The solution was stirred for 30 min before being transferred into 50 ml autoclave and kept at 180 °C for 12 h. The white sample powder was formed as the final product in the autoclave. The powder samples were then repeatedly washed with DI water and ethanol followed by drying in room ambient for 24 h.

Characterization was carried out with the samples at room temperature. Samples were characterized using scanning electron microscopy (SEM, not shown) and XRD. The diffraction measurements were carried out using a Rigaku Ultima III diffractometer with Cu-Kα radiation. PL studies were performed with a custom setup. Near UV excitation was produced by an argon-ion laser at $\lambda_{ex} = 363.8$ nm. Emission spectra were dispersed using a scanning spectrometer and detected with a cooled photomultiplier tube. PLE measurements were performed with a commercial spectrofluorimeter (PTI C61/2000 m Lawrenceville, NJ). For these measurements, powder samples were suspended in DI water in quartz cuvettes under constant stirring. All PLE spectra were obtained monitoring the red Eu^{3+} emission at wavelength $\lambda_{em} = 611$ nm. The separately measured water background was negligible.

III. X-RAY DIFFRACTION

XRD data are shown for each sample in Fig. 1(a). Each diffraction pattern is similar confirming consistent crystal structure for all samples. In Fig. 1(b), we summarize the 2θ peak positions as a function of Tb^{3+} concentration in the sample preparation. Clear from our data is a dependence in each diffraction angle with increasing Tb^{3+} content. The presence of this trend corresponds to an overall expansion in the lattice constant and confirms the expected Tb^{3+} is incorporated into the YBO_3 crystal structure during growth. The position of the XRD lines is an indication of this concentration. However, we

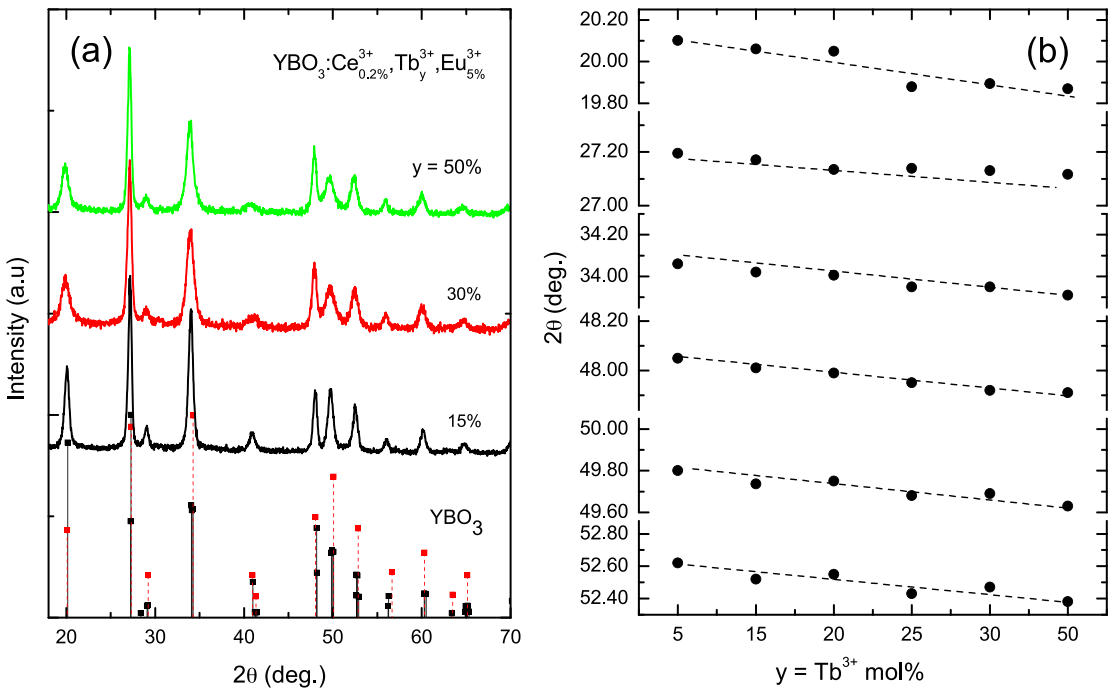

FIG. 1. (a) XRD patterns of $YBO_3:Ce^{3+}{}_{0.2\%},Tb^{3+}{}_{y},Eu^{3+}{}_{5\%}$ (y = 15%–50%) samples. The XRD peak positions of monoclinic (black symbols, PDF# 01-073-7388) and hexagonal (red symbols, PDF# 16-0277) YBO_3 crystal structure are included. (b) The variation of 2θ peak positions for intense bands with Tb^{3+} dopant concentration. Dotted lines are a guide to the eye.

note that the trend is not smooth, particularly for the 25% and 30% Tb^{3+} data. Since a monotonic dependence is expected with the dopant content, we consider the XRD data to be a better indicator of Tb^{3+} concentration than those based on the preparation conditions. Line widths were analyzed according to Scherrer's formula yielding a nanocrystal size of ~30 nm; no trend was observed with doping concentration.

IV. PHOTOLUMINESCENCE EXCITATION AND EMISSION SPECTROSCOPY

The terbium concentration is found to affect the optical properties of our materials. Figure 2 presents PLE (a–g) and corresponding PL (A–G) spectra of YBO_3:$Ce^{3+}_{0.2\%}$,Tb^{3+}_{y},$Eu^{3+}_{5\%}$ for samples with varying y from 5% to 50%. Intensities are scaled for each sample, so that the PLE intensity at $\lambda_{ex} = 363.8$ nm ($\lambda_{em} = 611$ nm) matches the PL intensity at $\lambda_{em} = 611$ nm ($\lambda_{ex} = 363.8$ nm) and are offset vertically for clarity. The PLE spectrum of YBO_3:Eu^{3+} is also included as a reference to help identify the effects of Tb^{3+} concentration on the excitation intensities of YBO_3:Ce^{3+},Tb^{3+},Eu^{3+} in the near UV region.

Specific bands are present in the PL spectrum, e.g., Fig. 2 spectrum A, related to the Ce^{3+}, Tb^{3+}, and Eu^{3+} ions in

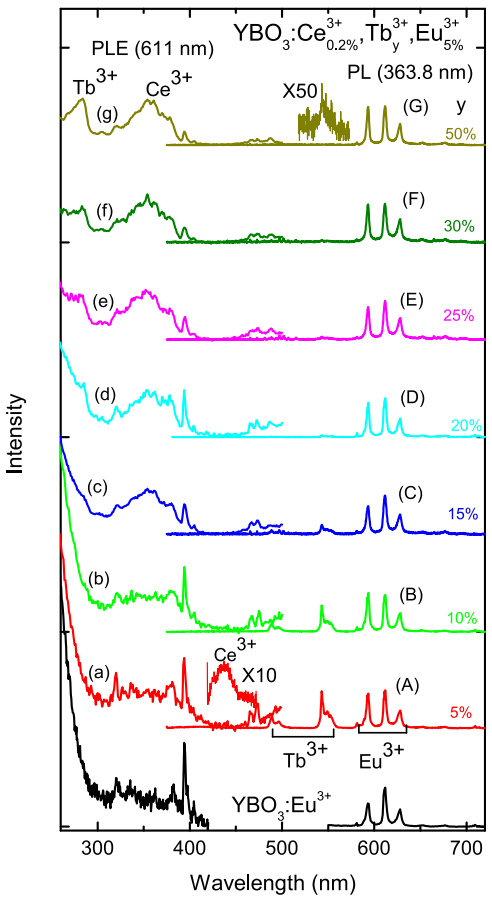

FIG. 2. (a–g) and (A–G) are PLE (monitoring 611 nm) and PL ($\lambda_{ex} = 363.8$ nm) spectra, respectively, of YBO_3:$Ce^{3+}_{0.2\%}$,Tb^{3+}_{y},$Eu^{3+}_{5\%}$ (y = 5%–50%) samples. The weak emission of Ce^{3+} and Tb^{3+} is magnified for clarity in (A) and (G), respectively. The PLE and PL spectra of YBO_3:Eu^{3+} are included as references to indentify the effect of Tb^{3+} ions on excitation states in near UV and emission of samples.

YBO_3:$Ce^{3+}_{0.2\%}$,$Tb^{3+}_{5\%}$,$Eu^{3+}_{5\%}$. The weak emission band from 370 to 430 nm is associated with 5*d*–4*f* states in Ce^{3+}.[7,8] The main Tb^{3+} emission peaks are at wavelengths 488 and 545 nm and originate from $^5D_4$-^7F_J (J = 6, 5) transitions.[9,10] The 591 nm orange (O) and 611 and 627 nm red (R) bands from Eu^{3+} belong to allowed magnetic dipole $^5D_0$-$^7F_1$ and forbidden electric dipole $^5D_0$-$^7F_2$ transitions, respectively. With an increase in the Tb^{3+} concentration to 10%, the Ce^{3+}-related emission is no longer observed. Additionally, the Tb^{3+} emission bands decrease relative to Eu^{3+} emission in the PL spectra as shown in Fig. 2, spectrum B. This trend continues with increasing Tb^{3+} content with only a trace PL band seen at y = 50%. We also note that the R/O ratio for the Eu^{3+} emission varies with terbium concentration. We return to this point later.

The decrease in PL intensities of Ce^{3+} and Tb^{3+} bands relative to Eu^{3+} emission may be due to ET from $Ce^{3+} \rightarrow Tb^{3+}$ and $Tb^{3+} \rightarrow Eu^{3+}$. It has been previously reported that the Ce^{3+} ions do not directly transfer energy to the Eu^{3+} ions in YBO_3 host matrix.[11] Moreover, the luminescence from the Eu^{3+} and Ce^{3+} ions is quenched due to the MMCT effect.[12] The addition of Gd^{3+} ions to YF_3 has been shown to mediate transfer of electrons from Ce^{3+} to Eu^{3+} and to negate the MMCT quenching.[12]

ET from $Ce^{3+} \rightarrow Tb^{3+} \rightarrow Eu^{3+}$ in YBO_3 may be studied using PLE by excitation of the Ce^{3+} and Tb^{3+} ions while monitoring emission from the Eu^{3+} color centers. The PLE spectrum, for YBO_3:$Ce^{3+}_{0.2\%}$,$Tb^{3+}_{5\%}$,$Eu^{3+}_{5\%}$ in Fig. 2, spectrum a, is similar to that of YBO_3:Eu^{3+}. The sample exhibits an intense broad deep-UV band near 241 nm (not shown) and weak intensity states in the range 310–390 nm. The deep UV feature is close to the excitation band of $O \rightarrow Eu$ charge transfer states of YBO_3:Eu^{3+}.[13,14] This feature is observed in the PLE spectrum of all samples studied here, although we see narrowing at higher Tb^{3+} concentration possibly due to the presence of a terbium-related absorption at 239 nm.[8,14] The excitation intensity in the range 310–390 nm is slightly increased with 10% Tb^{3+} content in Fig. 2 spectrum b. We conclude that low Tb^{3+} concentration does not effectively transfer energy from Ce^{3+} to Eu^{3+}. As Tb^{3+} concentration is further increased to 15% in spectrum c of Fig. 2, significant changes are observed. A weak shoulder appears near 285 nm and the near UV band from 310–390 nm increases in strength. Previous work has identified the 285 nm feature and the near UV band (310–390 nm) in the excitation spectrum to absorption by the Tb^{3+} to Ce^{3+} color centers, respectively.[2,7,8]

These Tb^{3+} and Ce^{3+} excitation bands in the PLE spectra for Eu^{3+}-related emission, and the quenching which occurs when only Ce^{3+} and Eu^{3+} are present in the YBO_3, indicate that energy transfer is taking place between the dopants according to $Ce^{3+} \rightarrow Tb^{3+} \rightarrow Eu^{3+}$ and $Tb^{3+} \rightarrow Eu^{3+}$. Because the Ce^{3+} and Tb^{3+} PL intensities are simultaneously decreasing relative to the Eu^{3+} emission, we conclude that the ET mechanism is affecting the emission from these color centers in Fig. 2 spectrum C. The intensity of the PLE bands at 285 nm and near the UV range 310–390 nm are improved further with higher Tb^{3+} content (y = 20%–50%) in Fig. 2, spectra d–g. The emission intensity of Tb^{3+} further decreases

relative to Eu^{3+} in the PL spectra D–G in Fig. 2. These trends further support the ET between dopants. It has been suggested that the Tb^{3+} ions form a Tb^{3+}-Tb^{3+} energy migration chain, denoted $(Tb^{3+})_n$, at higher Tb^{3+} concentrations. These chains transfer energy from Ce^{3+} to Eu^{3+} ions minimizing the MMCT effect between these two ions.[15] The strongest Tb^{3+} (285 nm) and Ce^{3+} (310–390 nm) excitation bands observed in our data are at high Tb^{3+} content (y = 50%), indicating effective ET from Ce^{3+} to Eu^{3+} at these levels and in agreement with the Tb^{3+} energy migration chain hypothesis.

V. R/O RATIO

To see the effect of the Eu^{3+} concentration on the $Ce^{3+} \rightarrow (Tb^{3+})_n \rightarrow Eu^{3+}$ energy migration chain, we decreased the concentration of Eu^{3+} from 5% to 1% keeping Ce^{3+} and Tb^{3+} fixed at 0.2% and 50%, respectively. In Fig. 3, we show the PLE and PL spectra, obtained under identical conditions as the data in Fig. 2, but without normalizing the measured intensities. We observed an increase in PLE intensities in the near UV region, and PL intensities in Fig. 3, for the sample with lower (1%) Eu^{3+} concentration. This may be due to reduced MMCT quenching effect between Eu^{3+} and Ce^{3+} ions at 1% when compared to the higher 5% concentration. In both cases, we obtain a high R/O intensity ratio (611 and 627 nm–591 nm), although we note that this is higher in the 5% Eu^{3+} sample than for 1%. Systematic studies varying the europium content are needed to optimize the R/O ratio.

It is interesting that the R/O ratio is varied across the samples in the A–G PL spectra in Figure 2 for fixed Eu^{3+} content. In all cases, the R/O ratios are greater than unity (Table I). In the YBO_3:$Ce^{3+}_{0.2\%}$,$Tb^{3+}_{50\%}$,$Eu^{3+}_{5\%}$ sample, for which we observe strong PLE in the near UV range, we obtain a R/O ratio of 1.68. The best R/O in this series of samples is for YBO_3:$Ce^{3+}_{0.2\%}$,$Tb^{3+}_{15\%}$,$Eu^{3+}_{5\%}$ for which we report 2.09. The R/O ratio obtained here is higher than the reported YBO_3:Ce^{3+},Tb^{3+},Eu^{3+} phosphor material using

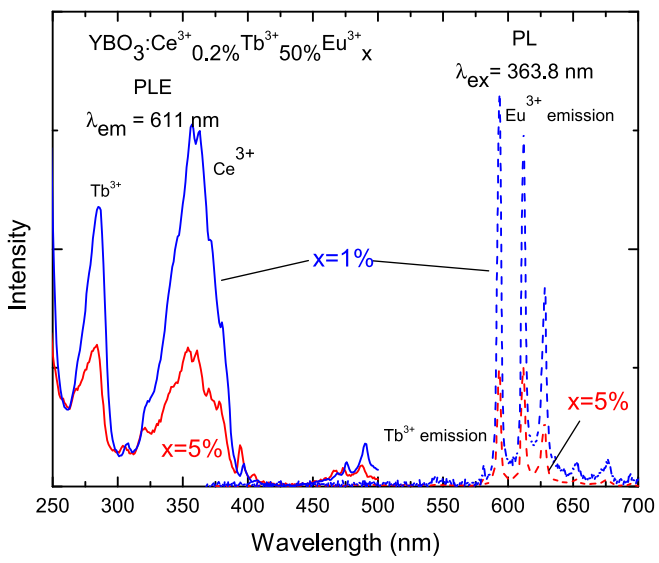

FIG. 3. PLE (monitoring 611 nm) and PL ($\lambda_{ex} = 363.8$ nm) spectra of YBO_3:$Ce_{0.2\%}$,$Tb_{50\%}$,Eu_x samples with x = 1% and 5%.

TABLE I. The R/O ratio in the PL spectra of YBO_3:Ce^{3+},Tb^{3+},Eu^{3+} samples.

Tb^{3+} (mol. %)	Ce^{3+}, Eu^{3+} (mol. %)	R/O ratio
5	0.2, 5	1.68
10	0.2, 5	1.54
15	0.2, 5	2.09
20	0.2, 5	1.91
25	0.2, 5	1.89
30	0.2, 5	1.70
50	0.2, 5	1.68
50	0.2, 1	1.34

360 nm excitation,[2] i.e., in the Ce^{3+} absorption band. Of the three YBO_3 dopant ions studied here—Ce^{3+}, Tb^{3+}, and Eu^{3+}—prior work has only addressed the sensitivity of the Eu^{3+} emission to the local structural environment in the host matrix.[5,13,16] Due to this sensitivity, the Eu^{3+} has been used to infer structural information about the YBO_3 host matrix.[16] If the Eu^{3+} ions lack inversion symmetry in the host matrix, then the forbidden electric dipole processes can be allowed according to Judd-Ofelt theory. We may then observe higher PL intensities from the red (611 and 627 nm) transitions compared to orange (591 nm). The varied R/O ratio in the PL spectra may suggest that the structural environment around the Eu^{3+} ions varies from sample to sample. This variation may be related to the Tb^{3+} dopant concentration in the YBO_3 crystal structure, through factors such as changes in bond angles and lengths surrounding the Eu^{3+} ions, thereby influencing the emission.

VI. RAMAN SPECTROSCOPY

To check for structural variations in our samples, beyond what is available in XRD, we carried out vibrational Raman studies. Figure 4(a) shows the Raman spectra of YBO_3:$Ce^{3+}_{0.2\%}$,Tb^{3+}_{y},$Eu^{3+}_{5\%}$ (y = 5% to 50%) and YBO_3:$Ce^{3+}_{0.2\%}$,$Tb^{3+}_{50\%}$,$Eu^{3+}_{1\%}$ samples. The peaks in the range 250–1150 cm^{-1} are associated with different vibrational modes of the B_3O_9 ring structure in the YBO_3 crystal. The TB, TS, ring bending (RB), and ring stretching (RS) mode assignments are included in Fig. 4(a) according to previous investigators.[17] The TB and TS bands are particularly important in our study because they carry information about terminal oxygen atoms in the B_3O_9 rings which comprise the bent B-O-lanthanide structure,[18] where the lanthanide is the Y cation in the YBO_3 crystal structure and corresponds to the substitutional dopant site in our samples. Variations in the TB and TS vibrations are expected to carry information about the local structure of the yttrium ions. Consequently, their behavior may influence the emission, especially of the Eu^{3+} dopant, since europium substitutes for yttrium in YBO_3. We note that the majority of the Raman bands do not show a systematic deviation with terbium concentration. However, the TB bands near 257 and 427 cm^{-1}, and TS features, in 950–1100 cm^{-1} range,[13,19,20] are seen to vary.

The TB peak position near 427 cm^{-1} is observed to blue shift with increasing Tb^{3+} ion concentration. This is evident in the series of spectra in Fig. 4(a) and summarized in

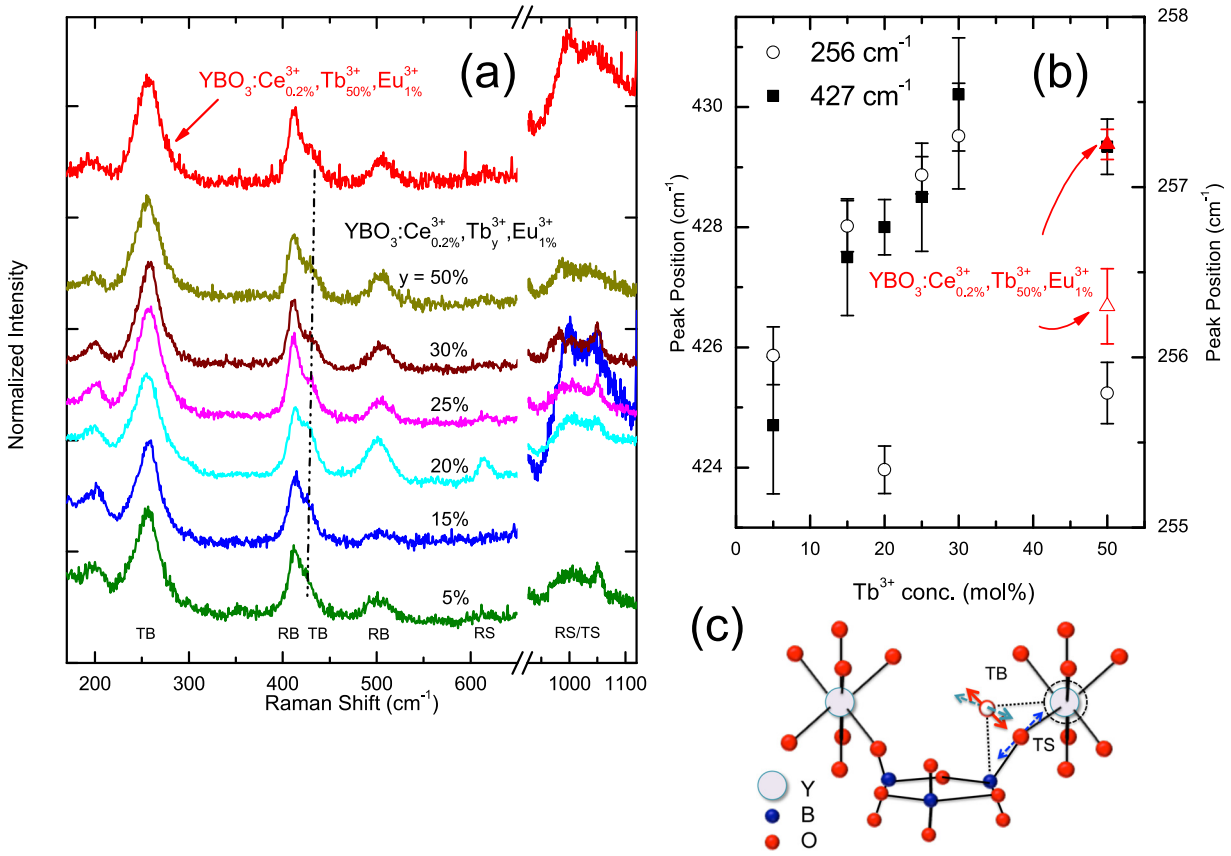

FIG. 4. (a) Raman spectra of YBO_3:$Ce^{3+}_{0.2\%}$,Tb^{3+}_{y},$Eu^{3+}_{5\%}$ (y = 5%–50%) samples. The dash line is a guide to track the oxygen TB band near 427 cm^{-1}. (b) Peak position of TB bands near nominal 256 cm^{-1} and 427 cm^{-1} with Tb^{3+} dopant concentration. The data points of YBO_3:$Ce^{3+}_{0.2\%}$,$Tb^{3+}_{50\%}$,$Eu^{3+}_{5\%}$ sample are also included (filled triangle 427 cm^{-1}, open triangle 256 cm^{-1}). (c) Depicts structure of YBO_3. Dashed ring surrounding one Y atom and dotted lines illustrate effect of size on oxygen (filled and open red circle) position. Included are TS vibrational displacement of the terminal oxygen (blue dashed line with arrows), and corresponding two TB modes in the B–O–lanthanide plane (red solid) and out of that plane (grey dotted). The TB modes are positioned at the displaced O atom for clarity.

Fig. 4(b) based on fits to the data. The intensity of this vibrational band also changes relative to RB band at ~412 cm^{-1}. It is weakest in the YBO_3:$Ce^{3+}_{0.2\%}$,$Tb^{3+}_{5\%}$,$Eu^{3+}_{5\%}$ sample and gradually grows in strength with higher Tb^{3+}. Based on this, we also examined the concentration dependence of the TB band near 255 cm^{-1}. A similar, but considerably weaker trend, is found in the data as summarized in Fig. 4(b). Based on this similar dependence, we attribute shifts in these vibrations to the same source. A plausible cause for the observed TB shift is the volume expansion implied by the XRD measurements with increasing Tb^{3+} incorporation. Lattice expansion will affect bond angles in this structure more than bond length, particularly for the tetrahedral BO_4 building blocks of the B–O ring structure. This expansion is expected to affect the terminal oxygen vibrations since terbium substitutes for the yttrium and these ions are bonded to the corresponding oxygen atoms.

Distortion near the lanthanide cation sites may produce a different effect on the TS and TB vibrations, as illustrated in Fig. 4(c) based on Ref. 21. There are two TB vibrations, one with displacement in the plane made by the B–O–lanthanide group and one perpendicular to that plane. The TS displacement is in the B–O–lanthanide plane. The oxygen displacements of these vibrations are illustrated in Fig. 4(c). For clarity, the TS mode is located at the nominal position of the oxygen atom in YBO_3, and the TB vibrations are displaced to the corresponding position following the illustrated (exaggerated) bond angle distortion. The TB mode will consequently be more strongly influenced by increases in the B–O–lanthanide bond angle. Because we expect the in-plane TB vibration to have a higher energy and to be more strongly affected by the volume deformation due to doping, we associate it with the Raman feature at 427 cm^{-1}. The band at 255 cm^{-1} may then be assigned to the TB vibration with displacement out of the B–O–lanthanide plane. The TS Raman bands in the range 900–1100 cm^{-1} also vary with terbium doping, although they do not show a particular trend with Tb^{3+} concentration. This may simply be due to the diminished interaction with the dopant as the distortion increases and the identity of TS and TB become blurred. We also see no dopant substitutional effect on the RB and RS bands. Since these modes are primarily internal to the ring structure they will be less affected by dopant perturbations due to their relative rigidity in the YBO_3 structure.

VII. SUMMARY

We have synthesized YBO_3:Eu^{3+} tri-doped with Ce^{3+} and Tb^{3+}, while systematically varying the terbium concentration. The XRD data in Fig. 1(b) shows a trend with Tb^{3+} concentration confirming the incorporation of this dopant in our

materials. The Tb^{3+} concentration influences PL emission when excited by near UV light. Increasing the Tb^{3+} concentration results in diminished PL from the Ce^{3+} and Tb^{3+} color centers for constant cerium and europium content, as seen in Fig. 2. The PL excitation bands related to both Ce^{3+} and Tb^{3+} increase in intensity for red emission from the Eu^{3+} with increasing terbium concentration. Results are consistent with a $Ce^{3+} \rightarrow (Tb^{3+})_n \rightarrow Eu^{3+}$ energy transfer scheme. A high R/O PL intensity ratio is obtained, ranging from 1.34 to 2.09. Several Raman bands in Fig. 4 show a systematic change, with Tb^{3+} concentration, in the TB mode related to the host lattice site which corresponds to yttrium position where the dopant ions substitute. The structural changes are interpreted as variations in the local neighborhood of these sites in the YBO_3:Ce^{3+},Tb^{3+},Eu^{3+} crystal structure. The Raman measurements confirm variations of the local order near the Eu^{3+} color centers induced by the terbium doping.

[1]A. A. Setlur, Electrochem. Soc. Interface **18**(4), 32 (2009), available at https://www.electrochem.org/dl/interface/wtr/wtr09/if_wtr09.htm.
[2]A. A. Setlur, Electrochem. Solid-State Lett. **15**, J25 (2012).
[3]B. R. Judd, Phys. Rev. **127**, 750 (1962).
[4]G. S. Ofelt, J. Chem. Phys. **37**, 511 (1962).
[5]S. Sohal, X. Zhang, V. V. Kuryatkov, J. Chaudhuri, and M. Holtz, Mater. Lett. **106**, 381 (2013).
[6]X. Zhang, A. Marathe, S. Sohal, M. Holtz, M. Davis, L. J. Hope-Weeks, and J. Chaudhuri, J. Mater. Chem. **22**, 6485 (2012).
[7]X. Zhao, X. Wang, B. Chen, W. Di, Q. Meng, and Y. Yang, Proc. SPIE **6030**, 60300N (2006).
[8]R. Sato, S. Takeshita, T. Isobe, T. Sawayama, and S. Niikura, ECS J. Solid State Sci. Technol. **1**, R163 (2012).
[9]L. Wang, L. Shi, N. Liao, H. Jia, P. Du, Z. Xi, and D. Jin, Mater. Chem. Phys. **119**, 490 (2010).
[10]P. K. Sharma, R. K. Dutta, and A. C. Pandey, J. Appl. Phys. **112**, 054321 (2012).
[11]G. Blasse and A. Bril, J. Chem. Phys. **47**, 1920 (1967).
[12]G. Blasse, Phys. Status Solidi A **75**, K41 (1983).
[13]Z. Wei, L. Sun, C. Liao, J. Yin, X. Jiang, and C. Yan, J. Phys. Chem. B **106**, 10610 (2002).
[14]Z. Xu, C. Li, Z. Cheng, C. Zhang, G. Li, C. Peng, and J. Lin, CrystEngComm. **12**, 549 (2010).
[15]D. Wen and J. Shi, Dalton Trans. **42**, 16621 (2013).
[16]G. Jia, P. A. Tanner, C.-K. Duan, and J. Dexpert-Ghys, J. Phys. Chem. C **114**, 2769 (2010).
[17]J. H. Denning and S. D. Ross, Spectrochim. Acta A **28**, 1775 (1972).
[18]J. Lin, D. Sheptyakov, Y. Wang, and P. Allenspach, Chem. Mater. **16**, 2418 (2004).
[19]Z. Zhang, Y. Zhang, X. Li, J. Xu, and Y. Huang, J. Alloys Compd. **455**, 280 (2008).
[20]G. Pan, H. Song, L. Yu, Z. Liu, X. Bai, Y. Lei, L. Fan, S. Lu, and X. Ren, J. Nanosci. Nanotechnol. **7**, 593 (2007).
[21]H. Shen, S. Feng, Y. Wang, Y. Gu, J. Zhou, H. Yang, G. Feng, L. Li, W. Wang, X. Liu, and D. Xu, J. Alloys Compd. **550**, 531 (2013).